British Society for Rheumatology

RHEUMATOLOGY

OXFORD

Clinical science

Development of a computed tomography calcium scoring technique for assessing calcinosis distribution, pattern and burden in dermatomyositis

Briana A. Cervantes[1,‡], **Prateek Gowda**[1,2,‡], **Lisa G. Rider** ⓘ [1], **Frederick W. Miller**[1],
Marcus Y. Chen[3,§], **Adam Schiffenbauer** ⓘ [1,*,§]

[1]Environmental Autoimmunity Group, Clinical Research Branch, National Institute of Environmental Health Sciences, National Institutes of Health, Bethesda, MD, USA
[2]National Institute of Biomedical Imaging and Bioengineering, National Institutes of Health, Bethesda, MD, USA
[3]Advanced Cardiovascular Imaging Laboratory, National Heart, Lung, and Blood Institute, National Institutes of Health, Bethesda, MD, USA
*Correspondence to: Adam Schiffenbauer, Environmental Autoimmunity Group, Clinical Research Branch, National Institute of Environmental and Health Sciences, National Institutes of Health, 10 Center Drive, Building 10, RM 6C432D, Bethesda, MD 20892, USA. E-mail: schiffenbauera2@niehs.nih.gov
‡B.A.C. and P.G. contributed equally.
§M.Y.C. and A.S. contributed equally.

Abstract

Objectives: To utilize whole-body CT imaging and calcium scoring techniques as tools for calcinosis assessment in a prospective cohort of patients with adult and juvenile dermatomyositis (DM and JDM, respectively).

Methods: Thirty-one patients (14 DM and 17 JDM) who fulfilled Bohan and Peter Classification criteria as probable or definite DM, the EULAR-ACR criteria for definite DM, and with calcinosis identified by physical examination or prior imaging studies were included. Non-contrast whole-body CT scans were obtained using low-dose radiation procedures. Scans were read qualitatively and quantitated. We calculated the sensitivity and specificity of calcinosis detection of physician physical exam against CT. We quantified calcinosis burden using the Agatston scoring technique.

Results: We identified five distinct calcinosis patterns: Clustered, Disjoint, Interfascial, Confluent and Fluid-filled. Novel locations of calcinosis were observed, including the cardiac tissue, pelvic and shoulder bursa, and the spermatic cord. Quantitative measures using Agatston scoring for calcinosis were used in regional distributions across the body. Physician physical exams had a sensitivity of 59% and a specificity of 90% compared with CT detection. A higher calcium score correlated with higher Physician Global Damage, Calcinosis Severity scores, and disease duration.

Conclusion: Whole-body CT scans and the Agatston scoring metric define distinct calcinosis patterns and provide novel insights relating to calcinosis in DM and JDM patients. Physicians' physical examinations underrepresented the presence of calcium. Calcium scoring of CT scans correlated with clinical measures, which suggests that this method may be used to assess calcinosis and follow its progression.

Keywords: calcinosis, CT, calcium scoring, DM, myositis

> **Rheumatology key messages**
> - Whole-body computed tomography scans detected calcinosis when performed with low radiation levels.
> - Physicians tended to detect less calcinosis than appreciated on computed tomography.
> - The Agatston scoring technique was successfully applied to calcinosis and correlated with physician calcinosis score.

Introduction

Calcinosis is a condition in which calcium salts are deposited in and around soft tissue, including the skin, subcutaneous fat, fascia and muscle. The calcification is dystrophic and occurs at normal serum calcium and phosphorous levels. Calcinosis is associated with many diseases including RA, scleroderma, SS, Werner's syndrome and calciphylaxis [1].

Adult and JDM syndromes (DM and JDM, respectively) are chronic inflammatory disorders characterized by progressive proximal muscle weakness and characteristic rashes [2]. Calcinosis is observed in up to 30% of DM patients and up to 70% of JDM patients [3]. There is significant morbidity associated with patients developing calcinosis, which often leads to functional disability and a

chronic course of disease [4]. Despite the existence of multiple treatment strategies for JDM, there are no proven effective therapies for calcinosis [5, 6].

Clinical assessment of calcinosis is usually conducted with a physical assessment or through plain X-rays. Prior X-ray studies have classified patterns of dystrophic calcinosis, referencing deep linear deposits, deep and superficial calcareal (also referred to as tumoral) masses and a lacy, reticular pattern [5, 7]. However, due to the two-dimensional nature of these X-ray images, much is still unknown about the spatial properties of calcification and the relative densities of the lesions. Other studies in patients with scleroderma calcinosis have aimed to measure calcinotic lesions using X-ray imaging compared with three-dimensional methods [8].

There is a need for a quantitative calcification metric to monitor patients over time, accurately assess responses to treatments, and correlate with other clinical parameters to improve our understanding of the causes of and best treatments for calcinosis. We explored the use of CT imaging for calcinosis in DM and JDM patients and adapted the Agatston score, a form of coronary artery calcification scoring, to quantify calcium burden as a novel tool for calcinosis quantification [9].

Patients and methods

Patient selection

Study subjects were recruited from a natural history study conducted at the National Institutes of Health (NIH) in Bethesda, MD (ClinicalTrials.gov identifier: NCT00017914), from November 2014 to December 2018. Inclusion criteria for the present study included probable or definite DM or JDM by Bohan and Peter criteria, definite criteria by EULAR-ACR classification, and suspicion of calcinosis by physical exam or prior imaging studies [10].

The study was conducted in accordance with the Declaration of Helsinki and the protocol was approved by a National Institutes Health Institutional Review Board (IRB). All patients provided written informed consent.

Whole-body CT scans

Patient scans were conducted on a 320-detector-row CT volumetric scanner (Aquilion One Vision or Genesis Edition, Canon Medical, Japan) at the NIH Clinical Center in Bethesda, MD with an 80-detector row helical acquisition and images were reconstructed into 5 mm axial slices with a 512×512 image matrix. Non-contrast whole-body scans were conducted from the top of the patient's head to the bottom of the feet, including the upper extremities. CT scans prior to October 2016 were acquired utilizing chest, abdomen and pelvis techniques with a standard image quality factor [image noise (S.D.) level of 12.5]. The CT system was upgraded in October 2016 and subsequent scans were performed utilizing an ultra-low radiation dose protocol (S.D. 30) [11–13]. Effective radiation doses were estimated using the dose length product reported by the scanner and multiplying by the conversion factor of 0.015 mSv/mGy cm for the chest, abdomen and pelvis.

CT subtype and region analysis

Subtype definitions of calcinosis categories were determined through a group meeting of authors P.G., L.G.R., F.W.M.,

M.Y.C. and A.S., where multiple CT images were shared and distinguishing characteristics of lesions were identified and discussed. This was done in the setting of review of the literature on calcinosis subtypes [7]. Author P.G. reviewed CT images and identified borderline cases and those that did not clearly fall into a subtype category. These cases were then re-reviewed by the panel for revision of the classification until there was 100% agreement on classification criteria.

All scans were read by the authors, P.G. and B.A.C., who were trained in identifying calcinosis lesions in CT images and verified by M.Y.C., a radiologist, all of whom were blinded to all clinical data. Any discrepancies were adjudicated, and a consensus resolution was reached at a second meeting.

Calcinosis lesions were assigned to segmented regions of the body using a predetermined rubric based on designated anatomic landmarks. These were: Head & Neck, Left and Right Distal upper extremities (UEs), Left and Right Proximal UEs, Chest, Abdomen, Pelvis, Left and Right Distal Lower Extremities (LEs), Left and Right Proximal LEs. Lesion location was recorded relative to organs, surrounding soft tissue and associated fluid collections.

Measurement of calcification from CT images of the heart was initially validated for risk stratification of cardiovascular risk. The Agatston method [9] uses a weighted sum of lesion area combined with density to yield a total score that describes the extent of calcification. This standard technique, which is commonly available on imaging workstations, enables the quantitative assessment of calcification and in this study applied to calcified regions outside the heart.

All quantitative analysis of the CT images was computed through the Vitrea Advanced software product (Vital Images, Version: 7.10.1.20, Minnetonka, MN, USA), using the conventional Agatston calcium scoring technique [9, 14]. Calcium scores >2 S.D. from the mean were excluded from analysis (two values excluded).

Laboratory and clinical methods

Patient sera were assessed for myositis-specific and associated autoantibodies by the Oklahoma Medical Research Foundation [15]. Rheumatologists A.S. and L.G.R. recorded locations and sizes of calcinosis lesions based on tactile examination. Measures of DM and JDM, including the Physician Global Activity and Damage, Physician Calcinosis Assessment, Health Assessment Questionnaire (HAQ)/Childhood Health Assessment Questionnaire (CHAQ), and Myositis Disease Activity Assessment Tool (MDAAT), were conducted by physicians A.S. and L.G.R. [16].

Statistical analysis

Statistical analyses were performed using SAS software, v9.4 (SAS Institute Inc., Cary, NC, USA). P-values <0.05 were considered significant.

Results

Characteristics of the study population

Thirty-one patients participated in the study: 14 patients with DM and 17 patients with JDM (seven of the JDM patients were adults at the time of CT scan). The demographics of the study participants are presented in Supplementary Table S1 (available at *Rheumatology* online). JDM and DM patients were similarly represented in race, sex, height, weight, BMI,

time since diagnosis, physician global disease activity, and damage. Only the anti-Ro autoantibodies were statistically different between both populations of patients ($P = 0.03$).

CT scan radiation dosing

Patients who underwent the standard protocol CT scans ($n = 17$) received an estimated effective radiation dose of 6.32 ± 3.62 mSv. After October 2016, whole-body CT scans conducted ($n = 14$) were performed utilizing ultra-low radiation dose techniques with an estimated effective radiation dose of 0.73 ± 0.68 mSv.

Identification of calcinosis subtypes

Assessment of CT cross-sectional images and 3D reconstructions of calcinosis from DM/JDM patients were evaluated for patterns and yielded five distinct subcategories from expert panel review. These subcategories were defined as: Clustered, Disjoint, Interfascial, Confluent and Fluid-filled (Fig. 1).

Clustered calcifications were formed in small, aggregate patterns. The clusters are comprised of individual lesions that presented <30 mm from the closest edge of the neighboring calcification (Fig. 1A). This pattern was also associated with scattered liquid calcifications (<130 Hounsfield units, HU) and was comprised of smaller calcinosis lesions (5 mm length) found in subcutaneous fat. This pattern most resembles the superficial calcareal type described by Blane *et al.* [7].

Interfascial lesions followed the cross-sectional geometry of tissue fascia. They were typically observed surrounding muscle bundles and the intersection between fat and skin, or fat and muscle in thin sheets (Fig. 1B). They were more likely to be found in deep tissue. These were similar to the deep linear type reported by Blane *et al.* [7].

Disjoint calcifications were singular, isolated calcifications, with a >30 mm separation from a neighboring lesion (Fig. 1C). They are typically larger than Clustered calcifications and present with smooth edges and are most common in the subcutaneous fat. These calcifications are located superficially in the skin and subcutaneous fat.

Confluent lesions were comprised of small, lacy-type calcifications and typically existed in fat tissue. They often presented in patients with the largest quantities of calcinosis. This pattern has been previously described by Blane *et al.* [7] as a deep linear calcareal or lacy pattern. However, CT imaging of these calcifications shows they are comprised of small, oblong calcifications, connecting in a linear fashion (Fig. 1D).

Fluid-filled lesions were isolated hollow lesions characterized by a liquid center (Fig. 1E). The fluid was identified by measuring an attenuation of <130 HU. Fluid-filled lesions were fluid-filled cores that could either be fully or partially surrounded by solid calcinosis. This seems most likely to have been previously classified as the calcareal subtype described by Blane *et al.* [7].

The number of patients exhibiting each type of lesion was as follows: 19 Clustered, seven Interfascial, four Disjoint, 12 Confluent and three Fluid-filled. Patients often exhibited multiple types of calcification. The most common combination was the Clustered and Interfascial type seen in seven patients. No relationship was seen between calcinosis subtype and disease duration, although this may be limited by small sample sizes.

Regional distribution and locations of calcinosis

The relative occurrence of calcinosis by CT was recorded across body regions (Supplementary Fig. S1, available at *Rheumatology* online). The regions of highest and lowest calcinosis occurrence were the proximal LEs (86.7%) and head and neck (40%), respectively. There were no significant differences in the regional distribution of calcinosis between DM and JDM.

Novel locations of calcinosis not previously reported included the spermatic cord ($n = 1$), the myocardium ($n = 1$), and the pelvic and shoulder bursa ($n = 2$). Calcifications were also observed in less reported locations within the breasts ($n = 5$) and genitals ($n = 3$) (Supplementary Fig. S2, available at *Rheumatology* online).

Performance characteristics of whole-body CT imaging

A 3D reconstruction of each CT scan was constructed to reveal the full extent and pattern of calcinosis (Supplementary Video Files and Placeholder, available at *Rheumatology* online). The reconstructed CT scan was used as a comparison against detection of calcinosis by physician evaluation (Fig. 2). The originally identified lesion locations were classified into a smaller number of larger areas for this comparison to physician evaluation. There was moderate agreement in detecting calcinosis in these larger body regions by either physical exam or CT scan ($\kappa = 0.45$, 95% confidence interval [95% CI] 0.38, 0.52) (Fig. 3D). Other than the proximal arms, the physician detected a lower occurrence of calcinosis
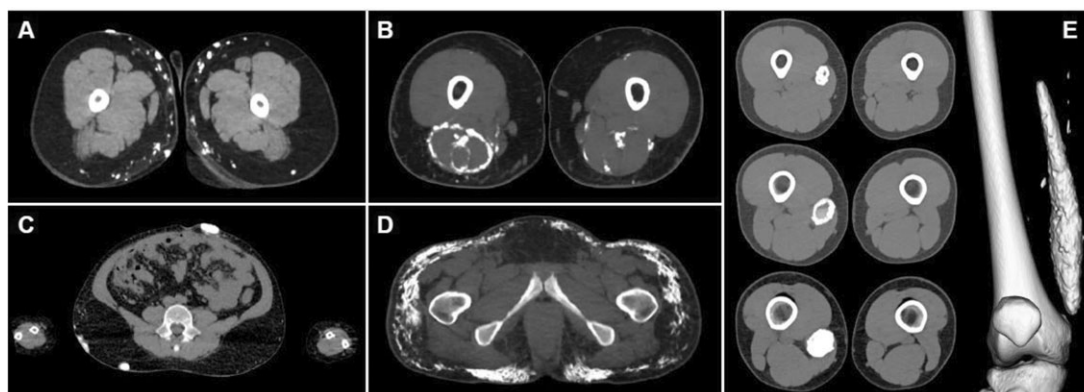

Figure 1. The major patterns of calcinosis. (**A**) Small, cluster pattern. (**B**) Fascial planar pattern. (**C**) Large, disjoint pattern. (**D**) Confluent pattern. (**E**) Fluid-filled capsule

Figure 2. CT scan comparison against 2D imaging and physician evaluation. (**A**) CT image allows better resolution of structure in 3D space. (**B**) Indicates a lacy pattern in 2D space. (**C**) Physician-detected calcinosis. (**D**) Photograph of bilateral legs. (**E**) 3D Reconstruction of CT scan on the same patient

in each body region category compared with the CT scan. This was especially evident in the pelvis and distal lower extremities. Considering the CT scan as a gold standard, the physician physical exam had a sensitivity of 59% (95% CI 53, 64) and a specificity of 90% (95% CI 87, 95) for detecting calcinosis.

Calcium scoring associations against disease parameters

Total average Agatston score, normalized by patient height, was 3128.52 ± 5868.52 (adult DM: 1741.93 ± 2347.21, JDM: 4630.67 ± 8024.76), with no difference by clinical subgroup (Fig. 3A). Agatston scores significantly correlated with the Physician Global Damage (Spearman $r = 0.80$, $P < 0.001$) (Fig. 3B) and the physician assessment of global calcinosis (Spearman $r = 0.65$, $P = <0.001$). Calcium score also significantly correlated with disease duration, as defined by the time since diagnosis of DM to the date of CT scan (Spearman $r = 0.69$, $P < 0.001$) (Fig. 3C). Calcium score and disease type, DM and JDM, were not significantly correlated ($W = 0.648$). Calcium score and Physician Global Activity had no significant correlation in our studies (Spearman $r = 0.34$, $P = 0.101$). Patient weight, BMI, MDAAT and CHAQ/HAQ did not significantly correlate with calcium score (Spearman $r = 0.01$, $P = 0.95$; $r = -0.03$, $P = 0.90$; $r = 0.21$, $P = 0.328$; $r = 0.26$, $P = 0.21$, respectively).

Discussion

This study demonstrates that whole-body CT provides information about calcinosis structure, distribution and quantification in DM and JDM patients. CT scans produce a 3D visualization of the structure and locations of calcinosis lesions across the body, including their relative position to other tissues. Furthermore, the Agatston score, which was originally developed to quantify the calcium burden of coronary artery plaque, provides a standard metric to assess the total amount of calcinosis in the patient with DM/JDM. In our study, we used CT scans to identify distinct subtypes of calcinosis that can be defined by their cluster pattern, shape and location relative to tissues. While some of our categorizations confirmed a prior typing of calcinosis based on plain radiographs [7], our descriptions revised existing definitions of calcinosis shapes. For example, 3D reconstruction of confluent calcinosis revealed a significantly different structure than previously described by 2D X-ray, which was described as having a lacy/reticular pattern with sharp connected segments of bone.

The calcinosis patterns we observed are not mutually exclusive, and often a single patient exhibited multiple types across their entire body. Further studies of these calcinosis subtypes may allow for better assessment of patient outcomes and may be found to correlate with other measures of disease activity, severity or phenotypes.
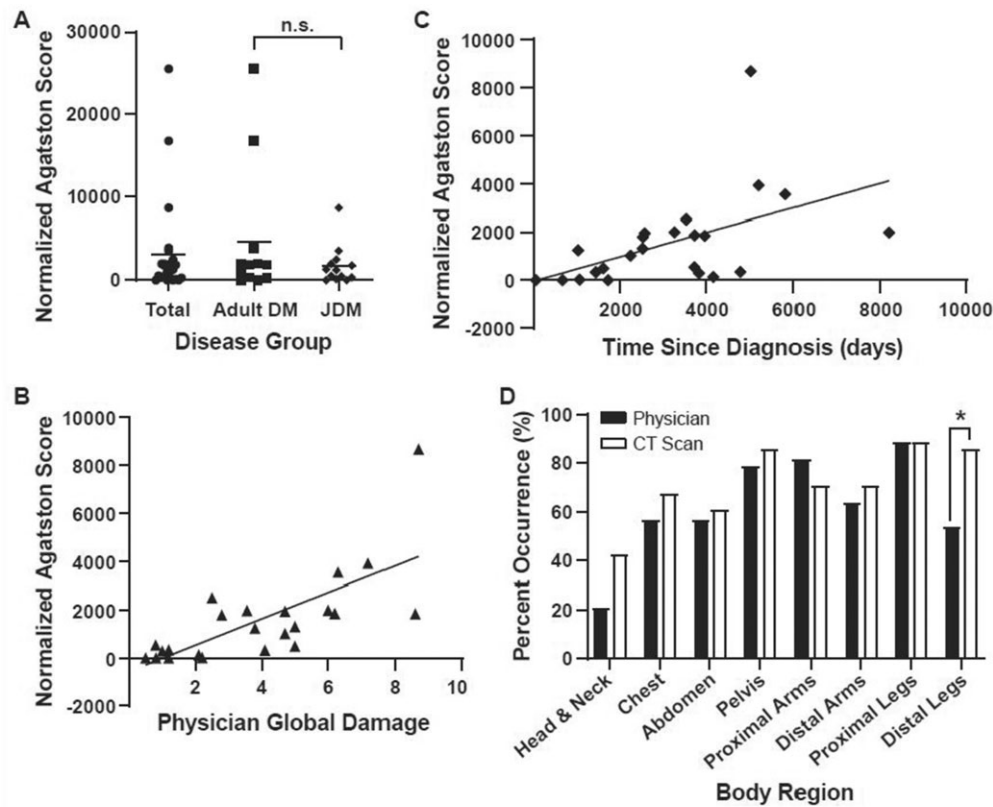
Figure 3. Calcium score by disease group, clinical metrics and detection between CT and physical examination. (**A**) Comparison of the height normalized calcium score (Agatston) across adult DM and JDM disease, W value = 0.644, n.s. (**B**) Height normalized calcium score (Agatston/cm) against physician measure of disease damage, Spearman: r = 0.80, $P < 0.001$. (**C**) Height normalized calcium score (Agatston/cm) against date of diagnosis to date of scan, Spearman: r = 0.69, $P = 0.001$. (**D**) Differences in calcinosis detection by body region across the cohort, Kappa = 0.45, Fisher's Exact: $*P < 0.05$; Distal legs

The most frequent sites of calcinosis we observed on CT imaging include the proximal and distal legs, pelvis, proximal arms, chest and abdomen, which are the locations previously frequently reported in the literature. However, we identified new calcinosis locations using CT imaging including the shoulder and pelvic bursa, cardiac tissue and the spermatic cord. The utility of the CT scan to reveal tissue location and structure can inform physicians when surgical removal of a lesion is being considered. Lesions of the Disjoint subtype, which are present in superficial locations such as skin or subcutaneous fat, may be ideal candidates for surgical removal.

The pelvis and lower extremities have an overall higher occurrence of calcinosis but are markedly underrepresented by physician exam. This regional distribution of calcinosis was similar between DM and JDM patients. Calcinosis is particularly difficult to identify in the pelvis using plain film X-ray approaches due to interference caused by the density of the pelvic bone. Underrepresentation of calcinosis in high-frequency areas may delay treatment options for patients and lead to increased calcinosis severity.

The Agatston score provides a standard metric to assess the total amount of calcinosis in the patient. Calcium burden correlated with measures of physician global damage and the duration of DM/JDM. However, calcium burden did not correlate with patient height, weight, BMI or measures of disease activity.

The CT scan provided an accurate measure of DM disease damage that can be used to supplement other clinical tools.

Radiation exposure must be considered because the FDA specifies a maximum annual research dose of 50 mSv (21 C.F.R. §361.1 2019). In our study, we transitioned to the ultra-low radiation dose techniques once available [11–13]. The ultra-low dose protocol (0.7 3 ±0.68 mSv) was significantly lower than the standard CT protocol radiation dose (6.3 2 ±3.62 mSv). Another study, using a low-dose CT protocol for imaging calcinosis in specific regions of the body had an average effective dose of 0.245 mSv for the chest alone [17]. In comparison to a chest X-ray, which is regularly performed in patients with DM and JDM, the ultra-low dose whole-body CT scan exposes patients to about seven times as much radiation, but images the entire body. This low radiation dose permits more frequent CT imaging. As a result, serial measurements can be performed that can provide insight into the rate of calcinosis volumetric change over time. A low-dose CT protocol also reduces the cumulative lifetime radiation in the adult and pediatric myositis populations, who may utilize repeated CT scans to assess efficacy of treatment. Further reduction of radiation dosage can be achieved using targeted CT scans to focus on areas of interest in patients who have previously completed a survey whole-body CT.

In this study, we were limited in our ability to analyse changes over time in calcinosis subtype and score because we did not perform serial scans. Another limitation was the inability to do simultaneous CT and X-ray images, the prior gold standard of imaging, due to radiation limits in our patients. The selection of our sample cohort focused on

patients with an established diagnosis of DM/JDM with previously documented calcinosis, which limits our ability to comment on those with very mild calcinosis.

Utilizing both the low radiation dose protocol and the Agatston score technique [9], this novel CT imaging approach provides a method to quantify calcinosis. Ultra-low dose whole-body CT detects the type and range of distribution of calcinosis structures to produce a safe and objective measurement of calcification.

Supplementary material

Supplementary material is available at *Rheumatology* online.

Data availability

The data underlying this article will be shared on reasonable request to the corresponding author.

References

1. Chung MP, Richardson C, Kirakossian D *et al.* Calcinosis biomarkers in adult and juvenile dermatomyositis. Autoimmun Rev 2020;19:102533.
2. Tansley SL, McHugh NJ, Wedderburn LR. Adult and juvenile dermatomyositis: are the distinct clinical features explained by our current understanding of serological subgroups and pathogenic mechanisms? Arthritis Res Ther 2013;15:211.
3. Dourmishev LA, Durmishev A. Dermatomyositis: advances in recognition, understanding, and management. Berlin: Springer, 2009.
4. Saini I, Kalaivani M, Kabra SK. Calcinosis in juvenile dermatomyositis: frequency, risk factors and outcome. Rheumatol Int 2016;36:961–5.
5. Orandi AB, Baszis KW, Dharnidharka VR *et al.* Assessment, classification and treatment of calcinosis as a complication of juvenile dermatomyositis: a survey of pediatric rheumatologists by the childhood arthritis and Rheumatology Research Alliance (CARRA). Pediatr Rheumatol 2017;15:71.
6. Traineau H, Aggarwal R, Monfort JB *et al.* Treatment of calcinosis cutis in systemic sclerosis and dermatomyositis: a review of the literature. J Am Acad Dermatol 2020;82:317–25.
7. Blane CE, White SJ, Braunstein EM, Bowyer SL, Sullivan DB. Patterns of calcification in childhood dermatomyositis. Am J Roentgenol 1984;142:397–400.
8. Hughes M, Hodgson R, Harris J *et al.* Imaging calcinosis in patients with systemic sclerosis by radiography, computerised tomography and magnetic resonance imaging. Semin Arthritis Rheum 2019;49:279–82.
9. Agatston AS, Janowitz WR, Hildner FJ *et al.* Quantification of coronary artery calcium using ultrafast computed tomography. J Am Coll Cardiol 1990;15:827–32.
10. Bohan A, Peter JB. Clinical presentation and diagnosis of polymyositis and Dermatomyositis. New Engl J Med 1975;292:344–7.
11. Hu-Wang E, Schuzer JL, Rollison S *et al.* Chest CT scan at radiation dose of a posteroanterior and lateral chest radiograph series. Chest 2019;155:528–33.
12. Choi AD, Leifer ES, Yu J *et al.* Prospective evaluation of the influence of iterative reconstruction on the reproducibility of coronary calcium quantification in reduced radiation dose 320 detector row CT. J Cardiovasc Comput Tomogr 2016;10:359–63.
13. Choi AD, Leifer ES, Yu JH *et al.* Reduced radiation dose with model based iterative reconstruction coronary artery calcium scoring. Eur J Radiol 2019;111:1–5.
14. Blaha MJ, Mortensen MB, Kianoush S, Tota-Maharaj R, Cainzos-Achirica M. Coronary artery calcium scoring: is it time for a change in methodology? JACC Cardiovasc Imaging 2017;10:923–37.
15. Targoff IN, Mamyrova G, Trieu EP *et al.* A novel autoantibody to a 155-KD protein is associated with dermatomyositis. Arthritis Rheum 2006;54:3682–9.
16. Rider LG, Werth VP, Huber AM *et al.* Measures of adult and juvenile dermatomyositis, polymyositis, and inclusion body myositis: physician and patient/parent global activity, Manual Muscle Testing (MMT), Health Assessment Questionnaire (HAQ)/ Childhood Health Assessment Questionnaire (C-HAQ). Arthritis Care Res 2011;63:S118–57.
17. Ibarra M, Rigsby C, Morgan GA *et al.* Monitoring change in volume of calcifications in juvenile idiopathic inflammatory Myopathy: a pilot study using low dose computed tomography. Pediatr Rheumatol 2016;14:64.